Pertanika J. Sci. & Technol. 30 (2): 1409 - 1419 (2022)

PERTANIKA JOURNALS

SCIENCE & TECHNOLOGY

Journal homepage: http://www.pertanika.upm.edu.my/

Evaluation of a Newly Designed Aerodisk for Cloud Seeding Prototype Rocket Drag Reduction

Ahmad Hussein Abdul Hamid[1], Zuraidah Salleh[1]*, Ambok Muhammad Izwan Ambok Suloh[1], Mohammad Juani Sujana[2], Mohd Shahar Saad[2] and Mohd Ismail Khamis[2]

[1]High Energy Material Research Laboratory (HEMREL), School of Mechanical Engineering, College of Engineering, Universiti Teknologi MARA, 40450 UiTM, Shah Alam, Selangor, Malaysia
[2]MTC Defense Sdn Bhd, Seksyen U8 Bukit Jelutong, 40150 Shah Alam, Selangor, Malaysia

ABSTRACT

The present work provides a detailed study of a cloud seeding prototype rocket's nose cone drag reduction strategy by adopting the Computational Fluid Dynamics (CFD) simulation method for solving compressible flow problems. Two different nose cone aerodisk models are simulated using OpenFOAM software: two hemisphere aerodisk and two spherically blunted tangent ogive aerodisk. The results are compared against a baseline case of the blunt nose cone. The solver used is first validated against published experimental data. It is observed that both aerodisk models significantly reduce the drag coefficient of the blunt nose cone with two spherically blunted tangent ogive aerodisk providing the lowest drag coefficient. Detailed comparison of the flow visualization in terms of temperature distribution and shock wave formation is also reported to determine its influence on aerodynamic drag. The present study generally reveals that two spherically blunted tangent ogive aerodisk is preferred over two hemisphere aerodisk for achieving greater drag reductions and lower heat load to the cloud seeding prototype rocket.

Keywords: Aerodisk, drag coefficient, nose cone, rocket, supersonic

ARTICLE INFO

Article history:
Received: 29 June 2021
Accepted: 18 August 2021
Published: 28 March 2022

DOI: https://doi.org/10.47836/pjst.30.2.31

E-mail addresses:
hussein@uitm.edu.my (Ahmad Hussein Abdul Hamid)
szuraidah@uitm.edu.my (Zuraidah Salleh)
ambokizwan@gmail.com (Ambok Muhammad Izwan Ambok Suloh)
juani@mtcgroup.com.my (Mohammad Juani Sujana)
shahar@mtcgroup.com.my (Mohd Shahar Saad)
ismail@mtcgroup.com.my (Mohd Ismail Khamis)
* Corresponding author

INTRODUCTION

For the past few decades, haze has afflicted Malaysia almost every year (Latif et al., 2018). As a result, the Malaysian government has to bear expensive costs to carry out cloud seeding processes once the Air Pollutant Index reaches a dangerous level (Haque, 2019). Seeding cloud using flare-carrying

ISSN: 0128-7680
e-ISSN: 2231-8526

rocket is considered an effective and cheaper alternative to an aircraft carrying and spraying salt solution (in wet seeding operation) or lighting flares (in dry seeding operation). The development of rockets for this particular purpose is currently undergoing in High Energy Material Research Lab (HEMREL), Universiti Teknologi MARA, Malaysia. Technology weather modification rockets have been in service for their relatively low operation cost and are less risky than conventional operations using aircraft. Therefore, this study investigates different aerodisk designs to determine the optimum nose cone geometry and parameters that result in minimum aerodynamic drag since drag reduction is necessary for improved performance of the cloud seeding rocket.

Various nose cone shapes have been investigated to reduce the aerodynamic drag in the design of high-speed aerodynamic vehicles such as rockets, missiles (e.g., intercontinental ballistic missiles or ICBMs) and space shuttles. It enhances its aerodynamic performance and reduces dynamic loading on the vehicle. Newer studies investigated different aerodisk designs to enhance drag reduction of the vehicle further. Other than that, aerodisks were also used as a pitot tube to measure the flight speed, providing a safety clearance for a more efficient warhead detonation in antitank projectiles and as probes to collect gas samples (Mikhail, 1991). The relevant literature on various nose cone shapes and aerodisk designs is presented below.

Generally, blunt geometries are preferred over slender ones for hypersonic vehicles, given the higher volumetric efficiency and adequate accommodation of onboard sensors and telemetry equipment (Shoemaker, 1990). This shape allows greater space for the payload to be fitted into the nose cone part. Narayan et al. (2018) did a comparative numerical study of the hypersonic flow past spherically blunted and parabolic nose cones at a Mach number of 5.8. Their study revealed that parabolic nose cones at higher fineness ratios are preferred over spherically blunted ones for achieving higher drag reduction and lower heating in hypersonic vehicles. The formation of shock waves plays a vital role in modifying the aerodynamic characteristic to achieve better nose cones performance. A relatively strong shockwave is replaced with a system of weaker oblique shock waves in the presence of an aerodisk fitted to the cylindrical body, which results in boundary layer separation and the emergence of a shear layer (Album, 1968). It was shown that the presence of conical shock wave and the recirculation region downstream of the shock wave results in lower pressure acting on the body surface and consequently lower drag and overall aerodynamic heating. However, Piland and Putland (1954) study revealed that at certain ranges of Mach number and Reynolds number, the aerodisks would not provide any further drag reduction. These findings were further supported by a more recent study where no further reduction in drag was observed for aerodisks with a length of more than four times the diameter of the forebody (Sebastian et al., 2016).

Menezes et al. (2003), Tahani et al. (2013), Deng et al. (2017), and Yadav et al. (2018) investigated different aerospike and aerodisk designs and their effectiveness on drag

reduction. Menezes et al. (2003) conducted experimental and numerical investigations of various forward-facing aerospikes on a large-angle blunt nose cone flying at a Mach number 5.75. They reported that blunt cone with flat-faced aerodisk spike is the most effective, followed by hemispherical aerodisk spike, flat-tipped spike, and sharp-tipped spike. Their findings are further supported by the more recent finding where the flat-faced disk can further reduce the drag coefficient of the nose cone by as much as 4% relative to the hemispherical aerodisk spike (Deng et al., 2017). Although the percentage drag reduction seems insignificant, the drag is reduced considerably given the anticipated flight velocity and that the drag is proportional to the square of flight velocity. Furthermore, the authors concluded that the flat aerodisk-tipped spike could encapsulate the vehicle forebody (the nose cone) under the recirculation region (or termed aerodynamic shadow) regardless of the spike length based on the measured heat transfer rate on the nose cone surface. Their observations are supported by experimental and numerical data, despite some discrepancies between them. The authors deduced the observed difference due to the assumption of laminar flow boundary conditions and the unsteady oscillations of the separation bubble.

Interestingly, Tahani et al. (2013) study showed that hemisphere aerodisk is more effective in reducing drag compared to flat-faced aerodisk. It contrasts with what has been previously reported (Menezes et al., 2003). It is likely due to the different spike length to nose cone base diameter ratio, L/D, investigated in both studies, i.e., $L/D = 1$ in the latter study and $L/D = 1.5$ and 2 in the former study. The authors reported that the overall drag is reduced with a longer aerospike due to increased separation region (a high-pressure region) downstream of the blunt-body. The authors also reported that the sharp-tipped spike performed worst relative to hemisphere aerodisk and flat-faced aerodisk, corroborating previous experimental and numerical findings (Menezes et al., 2003).

Deng et al. (2017) compared single flat-faced aerodisk and doubled flat-faced aerodisk with various spike lengths to nose cone base diameter ratios. They found that the angle of the reattachment point is dependent not only on the L/D ratio but also on the direction of the nose cone axis relative to the free stream (i.e., the angle of attack). When the axis of the nose cone is aligned with the free stream, the angle of the reattachment point increases with aerospike length, while the opposite trend is observed when the nose cone is at an angle of attack. They also concluded that a double flat-faced aerodisk is more effective in reducing aerodynamic drag than a single flat-faced aerodisk. They argued that the double flat-faced aerodisk produces a larger recirculation region than the single flat-faced aerodisk for angles of attach range between 0° and 12°, resulting in smaller local pressure near the nose cone and thus smaller pressure drag. This finding is corroborated by a more recent study, where Yadav et al. (2018) set up three different disk configurations: single-disk, two-disk and three-disk. They concluded that two-disk and three-disk configurations are the most effective. Still, the three-disk configuration is redundant because there is not much difference in drag reduction effectiveness compared to the two-disk configuration.

Although numerous works have been done on various shapes of aerospike, the performance of spherically blunted tangent ogive aerodisk has yet to be investigated. Aerodynamically speaking, this shape is more efficient than other shapes previously mentioned; hence it is an interesting candidate for the drag reduction aerodisk design. In the present study, the performance of two hemisphere aerodisk and two spherically blunted tangent ogive aerodisk was investigated, focusing on drag and thermal load reduction purposes. Prior to the study, the authors have performed validation work based on the work done by Menezes et al. (2003). The performance of the abovementioned aerodisks was evaluated at a freestream Mach number similar to that of the validating case, i.e., 5.75. The nose cones are assumed to be operating up to 1000m from sea level. The governing equations are solved using OpenFOAM (Weller et al., 1998), an open-source CFD code well known in the academic and industrial sector due to a broad range of fluid dynamics applications, no limitation for parallel computing and open source.

METHODOLOGY

The nose cone and aerodisks were modelled using CAD software then imported into the background mesh. The size of the background mesh is designed to neglect possible boundary effects. The geometrical dimensions of the baseline blunt nose cone and the other two aerodisks are depicted in Figure 1.

For this simulation, the mesh is generated using the native OpenFOAM meshing utility blockMesh and snappyHexMesh. BlockMesh uses the definition of vertices, blocks, edges, and faces to define the background mesh, while snappyHexMesh defines the layers of meshes in the vicinity of the body. The flow is treated as axisymmetric hence the domain is extruded into a 5° wedge geometry. This type of domain significantly reduces the number of cells and thus the computational resources required for solving the flow problems while preserving the solution accuracy given the nature of the flow.

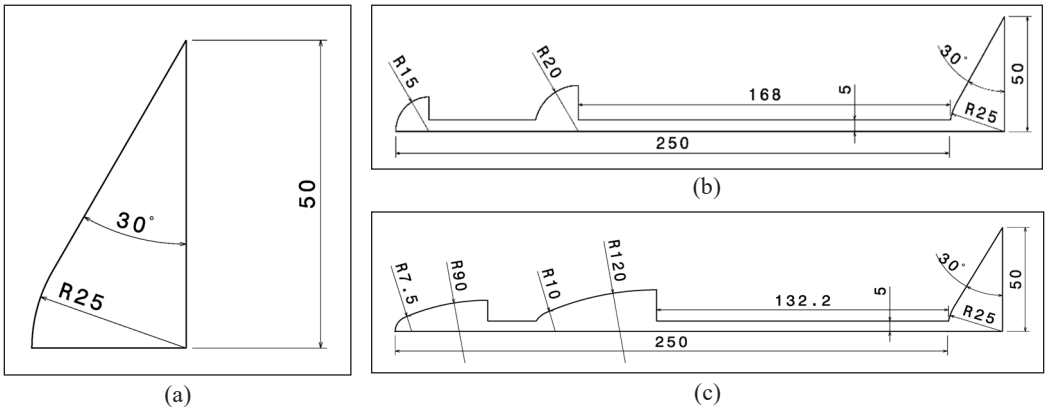

Figure 1. Geometrical dimensions of (a) blunt nose cone, (b) two hemisphere aerodisk and (c) two spherically blunted tangent ogive aerodisk

The domain is divided into six blocks that provide greater local refinement flexibility, as shown in Figure 2. Block 2 is the most critical region where the nose cone resides, and a high-velocity gradient is expected near its boundary. Therefore, block 2 will be the most refined compared to the other blocks. In this study, the turbulence is fully resolved via a fine mesh and small-time step. The time step is adaptable based on the condition of Courant number less than 0.6.

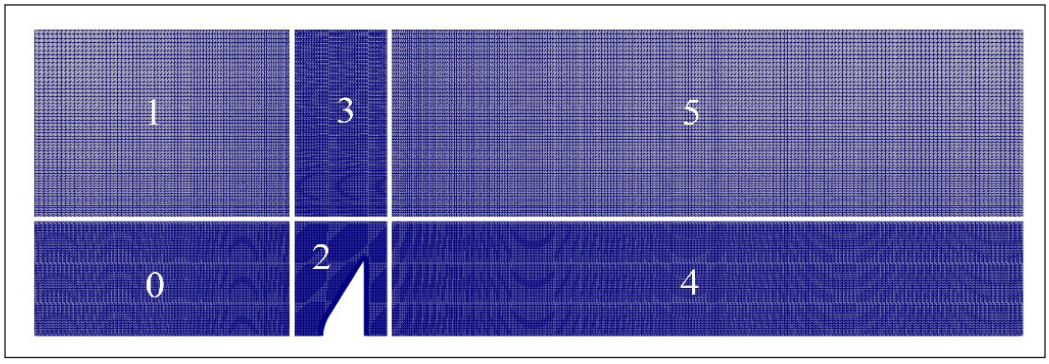

Figure 2. Baseline computational domain with local refinement near the nose cone

The velocity at the inlet boundary is set to uniform at 1400 m/s, which correspond to a freestream Mach number of 5.75, while the freestream pressure and temperature are set to be P = 425 Pa and T = 140 K, respectively. A cold wall case is assumed, where the nose cone and aerodisk walls temperature is set to be T = 300 K. This decision is made following the previous findings (Wood, 1962), where the spike temperature has a negligible effect on the separation angle. The thermophysical properties of the gas are specified in Table 1.

Table 1
Thermophysical properties of air at 1000 m above sea level

Properties	Value
Dynamic viscosity, μ (Nsm^{-2})	0
Prandtl number, Pr	1
Specific heat capacity, C_P (kJ/kg.K)	1.005
Molar mass, M ($gmol^{-1}$)	28.9

The compressible flow problems are solved using a density-based solver rhoCentralFoam, which uses the central-upwind schemes. Three equations, namely conservation of mass, momentum, and total energy were solved in an Eulerian frame of reference. The model used assumes the working gas behaves as perfect caloric gas. Thus, pressure is assumed to be proportional to the gas density and inversely proportional to the air compressibility. This solver was chosen as it has been reported to produce a minimal error compared with other solvers (Bondarev & Kuvshinnikov, 2018).

The data from the simulations were further analyzed using MATLAB codes to calculate the time-averaged quantities, such as the overall drag coefficient, for all the three models (blunt nose cone, two hemisphere aerodisk, two spherically blunted tangent ogive aerodisk).

Since, in all cases, the flow is time-dependent, the averaged data was calculated over a period where the data had reached a state of statistically stable (i.e., the transient regime is not counted for in the time-averaged calculations). This state is reached after a computing time of approximately 250 hours using a single core i7-8th generation Intel processor.

In order to validate the solver being used in the present study, the calculated time-averaged drag coefficient was compared against findings reported in Menezes et al. (2003). The comparison is summarized in Table 2.

Table 2
Results of blunt nose cone drag coefficient, C_D from different methods

Method	Blunt nose cone drag coefficient, C_D	Percentage difference compared to the experimental[a] result (%)
Present simulation	1.583	8.28
Experimental[a]	1.462	-
Numerical[a]	1.374	6.02

[a] Results reported in Menezes et al. (2003)

Based on this comparison, the present CFD simulation tends to overpredict the drag coefficient by approximately 8% relative to the reported experimental value (Menezes et al., 2003). Therefore, the present simulation is expected to produce drag coefficients of at most 8% error. This error is close to the error predicted by the previous authors (Menezes et al., 2003) using CFD simulation, which is 6% relative to their experimental values. Given the nature of the hypersonic flow that is highly turbulent, this error is likely due to the unresolved turbulence, particularly within the boundary layer. Resolving such small-scale turbulence would require high computing costs, and it is beyond the capacity of the present study.

RESULTS AND DISCUSSION

Temperature Fields

Analysis of temperature distribution around the nose cone is crucial since the temperature field determines the total heat transfer rate to the main body near the blunt-body. A higher temperature in the proximity of the rocket body means the body is subjected to the possibility of thermal failure if the temperature exceeds the material's critical temperature. Figure 3 compares the temperature fields around blunt nose cone, two hemispherical aerodisk and two spherically blunted aerodisk. It can be seen in Figure 3 that the temperature is highest in the proximity of the blunt nose cone when no aerodisk is installed. There is a very high-temperature region on the nose cone surface, marked by the bright yellow coloured region, and the temperature is as high as 1100K at the tip of the nose cone. It is also observed that a wide high-temperature region surrounds the nose cone, marked by the red coloured region.

However, the temperature is significantly reduced when aerodisks are fitted in front of the nose cone, and the high gradient temperature region is almost fully eliminated. This observation is due to a significant temperature reduction in the recirculation region [Figure 3(b)].

A concentrated high-temperature region was also formed downstream of the blunt nose cone, as shown in Figure 3(a). Interestingly, there is a significant difference in terms of downstream temperature filed between the two investigated aerodisks. In the case of two hemispherical aerodisk, temperature shear layers formed downstream of the nose cone while not observed in the two spherically blunted tangent ogive aerodisk cases.

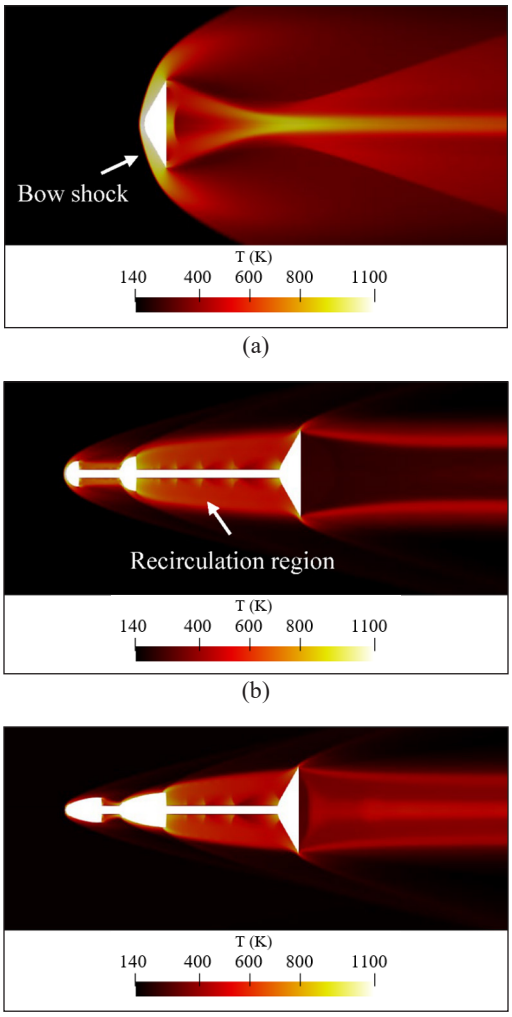

Figure 3. Temperature contours of (a) blunt nose cone, (b) two hemispherical aerodisk, and (c) two spherically blunted tangent ogive aerodisk. The temperature ranges from 140K (black) to 1100K (yellow).

Velocity Contour and Shock Wave Formation

The contours of velocity magnitude around blunt nose cone, two hemisphere aerodisk and two spherically blunted tangent ogive aerodisk are depicted in Figure 4.

In the case of a blunt nose cone, the hypersonic flow decelerates to the subsonic near the nose due to the formation of strong bow shock at a small distance upstream of the blunt cone. The flow then re-accelerates in the region downstream of the bow shock. The downstream flow is then converged towards the centreline, forming a weaker reflected shock [Figure 4(a)].

In the case of a nose cone fitted with an aerodisk, the strong bow shock is eliminated and is replaced with reattachment shock [Figure 4(b) and Figure 4(c)]. The two hemisphere aerodisk and two spherically blunted tangent ogive aerodisk have significantly changed the flow field around the nose cone. The shock waves that occurred for both aerodisk**s** are mainly oblique foreshock, which deflects the free stream away from the nose cone. Furthermore, the

nose cone is almost completely enveloped within the recirculation region, as shown in Figure 4(d). The recompression shock from the reattachment point on the shoulder of the nose cone is visible in Figure 4(d). It was reported that the rate of convective heat transfer on the nose cone increased significantly at the point of reattachment. Hence, it deserves attention when designing the nose cone (Menezes et al., 2003). It is also noted that the oblique shock in front of the two spherically blunted tangent ogive aerodisk is much weaker than its two hemisphere aerodisk counterparts.

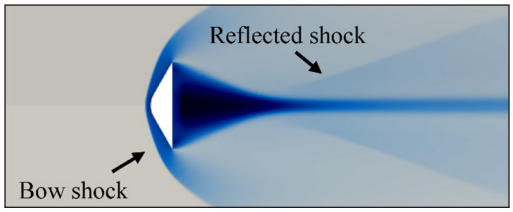

(a)

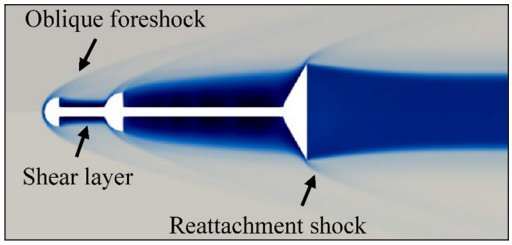

(b)

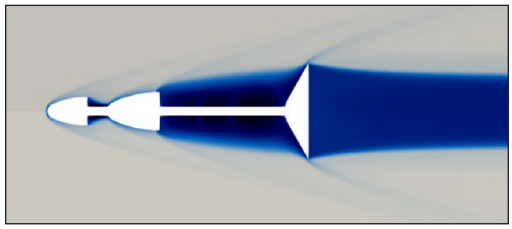

(c)

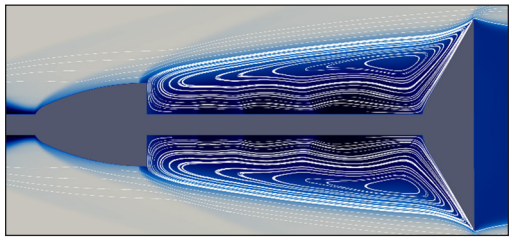

(d)

Figure 4. Comparison of streamwise (-z-direction) velocity of (a) blunt nose cone, (b) two hemispherical aerodisk and (c) two spherically blunted tangent ogive aerodisk. (d) shows the streamlines in the recirculation region of two spherically blunted tangent ogive aerodisk. The velocity ranges from -1400 m/s (grey) to 1200 m/s (black).

Drag Reduction

The coefficients of drag are calculated using the following Equation 1:

$$\bar{C_D} = \frac{1}{\frac{1}{2}\rho_\infty V_\infty^2 A(t_2 - t_1)} \int_{t_1}^{t_2} D(t)\, d(t) \quad [1]$$

where D is drag force (in N), which is the component of a force that is in the opposite direction of the free stream, ρ_∞ is the freestream density, in kg/m^3, V_∞ is the free stream velocity, in ms^{-1}, and A is the nose cone frontal area, in m^2. t_1 and t_2 are time range limits of which the averaged quantity is calculated. The time-averaged drag coefficients are summarized in Table 3. It is important to note that the time-averaged drag forces were determined after eliminating the transient part of the data to ensure the accuracy of the estimation.

As shown in Table 3, a substantial reduction in drag coefficient was achieved for aerodisk designs. For example, the two spherically blunted tangent ogive aerodisk has shown a significant reduction of approximately 90% in drag coefficient relative to the baseline case of the blunt nose cone. The drag reduction mechanism is associated with the

Table 3
Drag coefficient of baseline and aerodisks cases

Model	Blunt nose cone drag coefficient, C_D	Percentage reduction (%)
Blunt nose cone	1.583	-
Two hemisphere aerodisk	0.198	87.49
Two spherically blunted tangent ogive aerodisk	0.168	89.36

flow field behaviour over the aerodisk, i.e., the interaction of the shock waves, which is influenced by the configurations of the aerodisk. Furthermore, Tahani et al. (2013) argued that the increased separation region over the aerodisk and the normal shock in front of the aerodisk causes the drag to be reduced relative to the blunt nose cone.

It is also further noted that the two spherically blunted tangent ogive aerodisk gave slightly better drag reduction than the two hemisphere aerodisk (the difference in drag coefficient improvement is only 1.88%). It is likely due to the slender geometry design of the former aerodisk. Recent research done by Yadav et al. (2018) has reported a drag reduction as high as 74% using a three-disk spiked configuration. Depending on the design of the aerodisk, the contribution of the aerodisk to the total drag coefficient can be significant. For example, a two flat-faced disk aerodisk contributed almost 50% of the total drag coefficient, while a hemisphere disk contributed only approximately 18% (Deng et al., 2017).

CONCLUSION

The aerodynamic heating and forces of nose cones with two different aerodisk designs at hypersonic flow were numerically investigated. The aim was to understand the flow features, including shock wave formation, aerodynamic drag, and thermal loading. It was shown that the aerodisk fitted to a blunt nose cone has significantly altered the temperature distribution and shock wave formation around the nose cone. Furthermore, it was found that the two spherically blunted tangent ogive aerodisk can be a great drag reduction device, where a nose cone fitted with this aerodisk configuration has a drag of only 12% of the baseline case of the blunt nose cone. The main mechanism for the drag reduction is due to the separated region created by the aerodisk fitted to the nose cone. Furthermore, it is shown that the aerodisk has greatly lowered the heat load onto the nose cone.

ACKNOWLEDGEMENT

This publication was supported by the Strategic Research Partnership grants (100-RMC 5/3/SRP (020/2020) and 100-RMC 5/3/SRP PRI (024/2020)) and Micro-Industry Hub (MIH) Program (MIH-(005/2020)), a funded program under Universiti Teknologi MARA and MTC Engineering Sdn Bhd.

REFERENCES

Album, H. H. (1968). Regarding the utility of spiked blunt bodies. *Journal of Spacecraft and Rockets*, *5*(1), 112-114. https://doi.org/10.2514/3.29195

Bondarev, A. E., & Kuvshinnikov, A. E. (2018). Analysis of the accuracy of open FOAM solvers for the problem of supersonic flow around a cone. In Y. Shi, H. Fu, Y. Tian, V. V. Krzhizhanovskaya, M. H. Lees, J. Dongarra, & P. M. A. Sloot (Eds.), *International Conference on Computational Science* (pp. 221-230). Springer International Publishing.

Deng, F., Jiao, Z., Liang, B., Xie, F., & Qin, N. (2017). Spike effects on drag reduction for hypersonic lifting body. *Journal of Spacecraft and Rockets, 54*(6), 1185-1195. https://doi.org/10.2514/1.a33865

Haque, E. H. F. (2019). Govt spends RM80,000 for each cloud seeding operation. *New Straits Times*. https://www.nst.com.my/news/nation/2019/09/523244/govt-spends-rm80000-each-cloud-seeding-operation#:~:text=KUALA LUMPUR%3A The government incurs,Air Force's C-130 aircraft.

Latif, M. T., Othman, M., Idris, N., Juneng, L., Abdullah, A. M., Hamzah, W. P., Khan, M. F., Sulaiman, N. M. N., Jewaratnam, J., Aghamohammadi, N., Sahani, M., Xiang, C. J., Ahamad F., Amil, N., Darus, M., Varkkey, H., Tangang, F., & Jaafar, A. B. (2018). Impact of regional haze towards air quality in Malaysia: A review. *Atmospheric Environment*, *177*, 28-44. https://doi.org/10.1016/j.atmosenv.2018.01.002

Menezes, V., Saravanan, S., Jagadeesh, G., & Reddy, K. P. J. (2003). Experimental investigations of hypersonic flow over highly blunted cones with aerospikes. *AIAA Journal*, *41*(10), 1955-1966. https://doi.org/10.2514/2.1885

Mikhail, A. G. (1991). Spike-nosed projectiles: Computations and dual flow modes in supersonic flight. *Journal of Spacecraft and Rockets*, *28*(4), 418-424. https://doi.org/10.2514/3.26261

Narayan, A., Narayanan, S., & Kumar, R. (2018). Hypersonic flow past nose cones of different geometries: A comparative study. *Simulation*, *94*(8), 665-680. https://doi.org/10.1177/0037549717733051

Piland, R. O., & Putland, L. W. (1954). *Zero-lift drag of several conical and blunt nose shapes obtained in free flight at Mach numbers of 0.7 to 1.3*. National Advisory Committee for Aeronautics.

Sebastian, J. J., Suryan, A., & Kim, H. D. (2016). Numerical analysis of hypersonic flow past blunt bodies with aerospikes. *Journal of Spacecraft and Rockets*, *53*(4), 669-677. https://doi.org/10.2514/1.a33414

Shoemaker, J. (1990). Aerodynamic spike flowfields computed to select optimum configuration at Mach 2.5 with experimental validation. In *28th Aerospace Sciences Meeting* (p. 414). AIAA Inc.

Tahani, M., Karimi, M. S., Motlagh, A. M., & Mirmahdian, S. (2013). Numerical investigation of drag and heat reduction in hypersonic spiked blunt bodies. *Heat and Mass Transfer*, *49*(10), 1369-1384. https://doi.org/10.1007/s00231-013-1173-4

Weller, H. G., Tabor, G., Jasak, H., & Fureby, C. (1998). A tensorial approach to computational continuum mechanics using object-oriented techniques. *Computers in Physics*, *12*(6), 620-631. https://doi.org/10.1063/1.168744

Wood, C. J. (1962). Hypersonic flow over spiked cones. *Journal of Fluid Mechanics*, *12*(4), 614-624. https://doi.org/10.1017/S0022112062000427

Yadav, R., Bodavula, A., & Joshi, S. (2018). Numerical investigation of the effect of disk position on the aerodynamic heating and drag of a spiked blunt body in hypersonic flow. *The Aeronautical Journal*, *122*(1258), 1916-1942. https://doi.org/10.1017/aer.2018.109